Application of multi-quality parameter design in the optimization of underfilling process – a case study of a vehicle electronic module

Chien-Yi Huang
Department of Industrial Engineering and Management, National Taipei University of Technology, Taipei, Taiwan
Li-Cheng Shen and Ting-Hsuan Wu
Wistron NeWeb Corporation, Hsinchu, Taiwan, and
Christopher Greene
Binghamton University, Binghamton, New York, USA

Abstract

Purpose – This paper aims to discuss the key factors affecting the quality characteristics, such as the number of solder balls, the spread distance of residual underfill and the completion time of the underfilling.

Design/methodology/approach – The Taguchi method is applied to configure the orthogonal table and schedule and execute the experiment. In addition, principal components analysis is used to obtain the points. Then, based on gray relational analysis and the technique for order preference by similarity to ideal solution, the closeness between each quality characteristic and the ideal solution is adopted as the basis for evaluating the quality characteristics.

Findings – The optimal parameter combination is proposed, which includes 4 dispensing (11 mg/dispensing), a "half flow" interval state, 80°C preheating module PCB board and an L-shaped dispensing path and verification testing is performed.

Originality/value – For vehicles and handheld electronic products, solder joints that connect electronic components to printed circuit boards may be cracked due to collision, vibration or falling. Consequently, solder balls are closely surrounded and protected by the underfill to improve joint strength and resist external force factors, such as collision and vibration. This paper addresses the defects caused during the second reflow process of a vehicle electronic communication module after the underfilling process.

Keywords Technique for order preference by similarity to ideal solution (TOPSIS), Grey relational analysis (GRA), Taguchi method, Principal components analysis (PCA), Underfill process, Surface mount technology (SMT)

Paper type Research paper

1. Introduction

The global electronics industry is booming. At present, electronic products are designed to be light, thin, short and small; therefore, electronic assembly technology faces a growing number of market demands, including increasing the density of electrical breaker points, decreasing signal spacing and increasing the functional requirements (namely, input/output). A conventional peripheral array, such as a quad flat package (QFP), is adopted to place the chip functioning surface upwards onto the lead frame. Then, the signal is transferred from the chip to the lead frame by a wire bond, which is then packaged into an electronic component, to facilitate the subsequent bonding of the pins of the lead frame to the printed circuit board (PCB) via surface mount technology (SMT). In flip-chip technology, the chip's functioning surface is placed downwards on the substrate and the signal is connected to the substrate using solder bumps, as configured on the underside of the chip (Rangaraj *et al.*, 2017; Sylvestre *et al.*, 2014; Alander *et al.*, 2003). Area arrays, such as the ball grid array (BGA) and chip-scale package (CSP), use solder balls arranged on the substrate bottom to transfer the component signal to the PCB, effectively increasing the functional density of the packaged component.

The coefficients of thermal expansion (CTE) of the silicon chip and the substrate (FR-4 material) are 2.5 ppm/°C and 20 ppm/°C, respectively. For flip-chip on board (FCOB) technology, the CTEs of the two are not matched, thus, in the temperature cycle, the bonding bump between the chip and the substrate is subjected to thermal stress and maybe cracked. In addition, for vehicles and handheld electronic products, solder joints that connect electronic components to printed circuit boards (PCBs) may be broken due to collision, vibration or falling. The underfill contains epoxy resin, hardener, catalyst, filler and other additives (Zurcher *et al.*, 2018; Wu and Han, 2018; Shijian, 2000). Many investigators have examined the underfill encapsulation process (Ng *et al.*, 2019; Vincent and

The current issue and full text archive of this journal is available on Emerald Insight at: **https://www.emerald.com/insight/0954-0911.htm**

Soldering & Surface Mount Technology
33/2 (2021) 128–138
 [ISSN 0954-0911]
[DOI 10.1108/SSMT-05-2020-0016]

Received 3 May 2020
Revised 2 August 2020
14 August 2020
Accepted 14 August 2020

Wong, 1999; Nashrudin *et al.*, 2020). In the underfilling process, the underfill is injected on the edge of the electronic component (or chip) to fill the gap between the electronic component and the PCB (or chip and substrate) via the capillarity, which is then baked and cured to achieve the desired mechanical properties. Then, the solder balls (or the bump) are closely surrounded and protected by the underfill, to withstand the above mechanical external forces (or thermal stress) (Huang *et al.*, 2015; Jing Liu *et al.*, 2003; Cheng *et al.*, 2003). Li *et al.* (2016) run Taguchi experiments over the factor of gel injection quantity, time span between consecutive gel injection points, gel injection orders and board temperature to determine the optimum process parameter mix. Kuo *et al.* (2010) included the pad type, stencil opening, opening gap and power size as control factors in the experimental design.

1.1 Research motives

The current communication modules are mostly used in WiFi, Bluetooth, antennas, infrastructure networks, digital broadcasting, radar sensors and vehicle infotainment systems and are equipped with a central processing unit (CPU), memory, universal serial bus (USB), subscriber identity module (SIM) card and other functional components. In the production process, the communication module manufacturers first connect the memory component and the passive components to the module PCB through the SMT reflow soldering process and then, the underfilling process is performed on the memory component to improve the bonding strength and resist external forces, such as collision and vibration. A sketched image where all relevant parts in Figure 1(a); the appearance of the module and the cross-section of the memory component are shown in Figure 1(b). The module is then assembled onto the system PCB through a second reflow soldering process on the client-side (system manufacturer).

However, the above underfilling process may lead to the following defects: If the underfill contains air or the process parameters are improper, the underfill may not completely cover the solder balls, thus, forming a void [Figure 2(a)]. During the second reflow soldering process, the solder balls melt again and penetrate into the void, causing the risk of solder bead to short-circuit fault [Figure 2(b)]. While solder splashing during reflow soldering may also cause solder bead, our observation on the physical contact of the solder bead and the solder ball and the location of solder bead coincided with that of the underfill void indicate a high possibility that the formation of ball bead related to the underfill process. In addition, if the dispensing component (memory component) is too close to the surrounding passive component, and the underfill forms an excessively long residual spread distance on

Figure 1 Memory component in electronic communication module

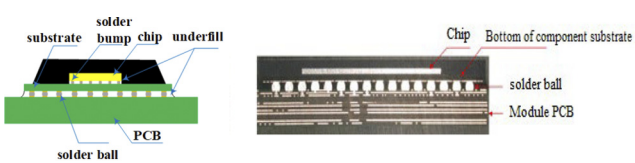

Notes: (a) Sketched image; (b) cross-section view

Figure 2 Defects in underfilling process

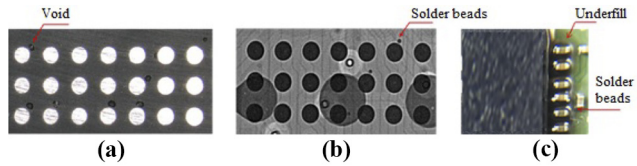

Notes: (a) Underfill void; (b) solder beads; (c) Dispensing component and surrounding passive component

the edge of the component, the passive component may adhere to the underfill. If the residual underfill does not completely cover the electrode solder of the passive component, the solder bead may be short-circuited due to the above mechanism [Figure 2(c)]. In addition, in the underfilling process, as the underfill may flow into the bottom of the component by a capillary phenomenon, improper process parameters often affect the completion time of the underfilling and an excessively long underfilling process will create a bottleneck workstation, affecting the overall production capacity.

1.2 Research purposes

To address the defects caused by the second reflow soldering process of the vehicle electronic communication module, after the underfilling process, this paper discusses the key factors affecting the quality characteristics, such as the number of solder beads, the spread distance of residual underfill and the completion time of the underfilling. The optimal processing parameter combination is determined by considering the multi-quality characteristics, to effectively improve the underfilling process and increase the processing yield.

2. Methodology

First, aimed at the vehicle communication module, the Taguchi method is applied to configure the orthogonal table and schedule and execute the experiment. In addition:

- principal components analysis is used to obtain the points. Then, based on gray relational analysis and
- the technique for order preference by similarity to the ideal solution (TOPSIS), the closeness between each quality characteristic and the ideal solution is adopted as the basis for evaluating the quality characteristics.

Finally, the optimal parameter combination is proposed and verification testing is performed. The research process is shown in Figure 3.

2.1 Characteristics of the research product

This study is aimed at the vehicle electronic communication module, which is 59.8 mm long and 50.2 mm wide. In this study, three CSP memory components, which are 14 mm long, 9 mm wide and 1.1 mm thick, are arranged on the module PCB. In addition, 96 solder balls are arranged on the bottom of the module (Figure 4). The gap between the bottom of the component substrate and the surface of the module PCB is 0.22 mm∼0.23 mm. In addition, this study uses underfill material with a glass transition temperature (Tg) of 140°C, a low coefficient of the thermal expansion of 21 ppm/°C and a viscosity

Figure 3 Research process

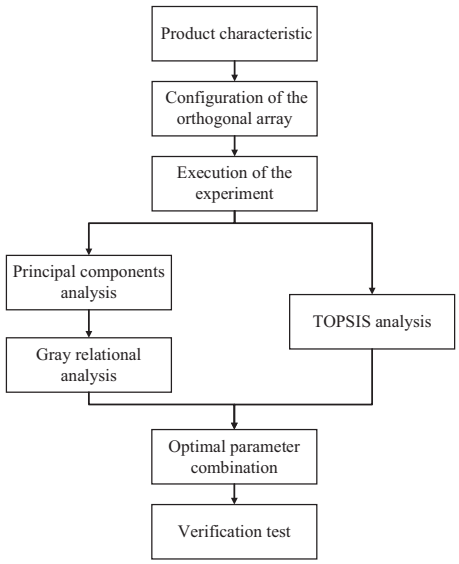

Figure 4 Configuration of solder balls on the bottom of the memory component

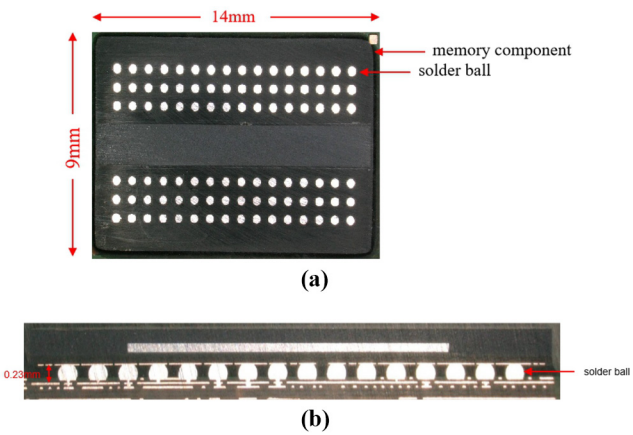

Notes: (a) Top view; (b) side view

at room temperature of 2.8e7 Pa·*s* (4,000 psi), making it less likely to cause splashing. To avoid condensation of water in the underfill due to exposure to the environment, which will change its viscosity, it should be warmed for 1 h before use (open bottle).

2.2 Quality characteristics

Aimed at the underfilling process, this paper considers the following quality characteristics, explained as follows.

- Number of solder beads: As mentioned above, the bottom void of the underfill may produce solder beads, thus, a short-circuit fault may occur to large solder beads or several solder beads, as they are closely located. This study uses an X-ray machine to detect the dispensing component and observe the number of solder beads produced [as shown in Figure 2(b)].
- Residual underfill spread distance (mm): Refers to the reverse spread distance, the underfilling or the footprint of the reservoir during the dispensing process (Figure 5). A smaller spread distance is beneficial to shorten the design distance between the dispensing component and the surrounding components, which reduces the size of the PCB and the end product.
- Completion time of underfilling (sec): Refers to the time required from the start of dispensing to the spread of the underfill to the component. In this experiment, a USB digital microscope with 1.3 million pixels and 200 times the three-dimensional micro-photo function was used to record the dispensing process and ensure the correctness of the data records.

2.3 Experimental design and execution

In this study, the Taguchi parameter design method was applied to determine the optimal parameter combination of the underfilling process and improve process stability.

2.4 Control factor and level

According to the results of the preliminary underfill experiments conducted in this research, the risk of a void occurrence is lower when the temperature of the dispensing head is set to 50°C, which creates a relatively stable process. In addition, when the starting point and the ending point of the dispensing path are located at component corners, the flow rate of the underfill along the component edge is higher. When the underfill on both sides converges, the air in the central part may be trapped to form a void, which is a "rewinding" phenomenon. Figure 6 is a simulated image from the top of transparent glass to illustrate the rewinding phenomenon. Therefore, a certain distance is reserved at the starting point and the ending point of subsequent dispensing paths to avoid creating a void. The total amount of required underfill, as estimated by equation (1), is 45 mg, which refers to the clearance volume between the component substrate and PCB minus the volume occupied by the solder balls, plus the underfill fillet, which is then multiplied by the specific gravity of the underfill 1.71. The above parameters are set as the fixed

Figure 5 Residual underfill spread distance

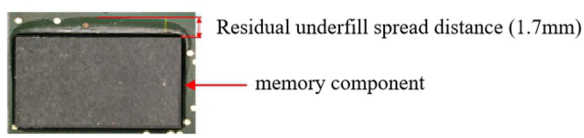

Figure 6 Rewinding phenomenon

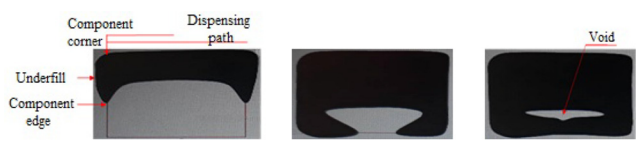

Notes: (a) Time 1; (b) Time 2; (c) Time 3

factors of this experiment. The experimental control factors and their levels are shown in Table 1 and described, as follows.

- *Dispensing:* As mentioned above, the total dispensing amount is fixed at 45mg. By dividing the dispensing, the amount of underfill can be reduced, which means that the residual underfill spread distance can be reduced; on the contrary, an increased number of dispensing can increase the completion time of the underfilling. This study considers 2 dispensing (22 mg/dispensing), 3 dispensing (15 mg/dispensing) and 4 dispensing (11 mg/dispensing).
- *Interval state:* During the dispensing process, the time of the next (second or more) dispensing start considers the state of the underfill, as formed by the previous dispensing. An excessive long dispensing interval may cause the underfill between the two adhesives to form air bubbles; while a short dispensing may cause the underfill to overflow to the surface of the component. The following three levels are considered in this study, "no waiting" refers to continuous multiple dispensing; "complete flow" refers to the start of the next dispensing when storage is completely depleted; "half flow" refers to the start of the next dispensing when half of the underfill storage is depleted.
- *Preheating module PCB board temperature:* By preheating the module PCB, a small amount of underfill contacts the module PCB with high thermal quality during the dispensing process. The temperature of the underfill increases instantly, the viscosity decreases and the fluidity increases. This study considers 70°C, 80°C and 90°C.
- *Dispensing path:* Proper dispensing path or extended underfill length may shorten the completion time of the underfilling (Kan, 1999). In this study, Short I-shaped, long I-shaped and L-shaped paths are considered (Figure 7).

$$V = L_c \times W_c \times g - \frac{4}{3}\pi r^3 N + \frac{1}{2}s^2 \times (L_c + W_c) \times 2 \quad (1)$$

where V is the total amount of underfill, L_c and Wc are the length and width of the memory component (L_c =14 mm, Wc = 9 mm), s is the gap between the memory component substrate and the PCB module (s = 0.23 mm) and N is the number of solder balls (N = 96).

2.5 Experimental configuration of the orthogonal array

In this study, four control factors with three levels are selected and the L_9 orthogonal table in the Taguchi experimental design is applied to schedule the experiment. The experimental configuration is shown in Table 2. In addition, each group of experiments is performed 3 times, which presents 3 observations. As mentioned above, a total of three memory components are arranged on the module PCB, that the relative position of the dispensing component on the module PCB is considered as a blocking factor, which means that the position of the same set of experimental dispensing components is evenly distributed to avoid the bias of the analysis results due to the position of the dispensing component. As the PCB heats up quickly and the natural cooling rate is uncertain, first, the parameter combination of the low PCB temperature (70°C) is executed and then, the parameter combination of the high PCB board temperature (90°C) is executed.

Table 1 Experimental control factors and their levels

Factor/level	Level 1	Level 2	Level 3
A. Dispensings	2	3	4
B. Interval states	No waiting	Half flow	Complete flow
C. PCB board temperature	70	80	90
D. Dispensing path	Short I-shaped	Long I-shaped	L-shaped

Figure 7 Dispensing path

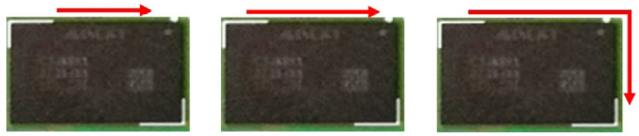

Notes: (a) Short I-shaped; (b) long I-shaped; (c) l-shaped

2.6 Preparation

First, the thermal couple is buried in the center of the module on the board and fixed by glue. Then, the PCB is placed in the bare space of the fixture to prevent the bottom surface of the solder ball from contacting the heating plate. In addition, the temperature of the dispensing machine is adjusted to the PCB board temperature of the preheating module; ensure that the component temperature is constant until dispensing is complete. The temperatures of two memory chips on the module are monitored using a thermal couple (Figure 8). The temperature profiles of the preheating module PCB and underfill curing are shown in Figure 9(a) and 9(b), respectively. While the constant 70°C is the PCB preheat temperature, the constant 140°C is the curing temperature during reflow. In addition, the underfill should be taken out of the freezer and warmed up for 1 h before use.

3. Analytical results

The experimental results are shown in Table 2. As the four quality characteristics are all smaller-the-better characteristics of Taguchi quality, the signal to noise ratio (SN) of each experimental group (parameter level combination) is calculated by equation (2), where y_i is the *i-th* measurement and n is the number of samples (n = 3). The Response table and factor effect of each quality characteristic, which is shown in Table 3 and Figure 10, respectively, to present the effect of different factors on the quality characteristics (SN). The larger SN value indicates a more desired factor level:

$$SN_{STB} = -10\log\left(\frac{1}{n}\sum_{i=1}^{n} y_i^2\right) \quad (2)$$

3.1 Principal components and gray relational analysis

As the ideal parameter combinations of the three quality characteristics are inconsistent, principal components analysis is used to linearly combine the relational quality characteristics and solve the multi-quality characteristic problem. Gray relational analysis is used to calculate the gray correlation

Table 2 Experimental configuration and result of L_9 orthogonal table

Experimental group	A Dispensing	B Interval states	C PCB board temperature	D Dispensing path	Response values	Observed values 1	2	3	SN
1	2	No waiting	70	Short I-shaped	Number of solder beads	42	4	14	28.19
					Underfill spread distance	1.69	1.71	1.68	−4.59
					Underfilling time	27	28	27	−28.74
2	2	Half flow	80	Long I-shaped	Number of solder beads	24	7	14	−24.37
					Underfill spread distance	1.45	1.40	1.45	−3.14
					Underfilling time	28	35	28	−29.69
3	2	Complete flow	90	L-shaped	Number of solder beads	22	47	39	−31.48
					Underfill spread distance	0.83	0.80	0.94	1.30
					Underfilling time	32	40	42	−31.65
4	3	No waiting	80	L-shaped	Number of solder beads	8	2	0	−13.55
					Underfill spread distance	1.03	0.96	1.04	−0.08
					Underfilling time	34	32	30	−30.11
5	3	Half flow	90	Short I-shaped	Number of solder beads	67	12	21	−32.28
					Underfill spread distance	1.05	1.16	1.11	−0.91
					Underfilling time	27	29	29	−29.05
6	3	Complete flow	70	Long I-shaped	Number of solder beads	55	13	0	−30.27
					Underfill spread distance	0.82	0.88	0.83	1.47
					Underfilling time	45	42	48	−33.08
7	4	No waiting	90	Long I-shaped	Number of solder beads	29	8	6	−24.97
					Underfill spread distance	1.46	1.51	1.40	−3.28
					Underfilling time	32	30	40	−30.70
8	4	Half flow	70	L-shaped	Number of solder beads	2	1	3	−6.69
					Underfill spread distance	0.69	0.65	0.68	3.41
					Underfilling time	37	40	42	−31.98
9	4	Complete flow	80	Short I-shaped	Number of solder beads	7	3	7	−15.52
					Underfill spread distance	0.85	0.97	0.90	0.85
					Underfilling time	64	67	73	−36.66

Figure 8 The locations for the temperature monitoring

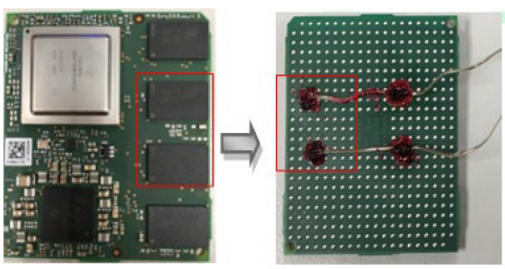

coefficient of each principal component, which is a single measure that objectively and effectively determines the optimal parameter combination (Vimal *et al.*, 2017; Huang *et al.*, 2016; Lu *et al.*, 2009; Chiang and Chang, 2006). The analysis steps are described, as follows:

Step 1: Standardize the original SN ratio matrix.

The m quality characteristics are used to evaluate the l parameter combinations and construct original matrix D. Specifically, SN_1, SN_2 and SN_3 are the numbers of solder beads, the residual underfill spread distance and the completion time of underfilling, respectively, and the results are shown in Table 4.

Equation (3) is used to normalize the SN ratio of each quality characteristic and obtain matrix $[S_{ij}]$, which is the normalized value of the SN ratio of the *j-th* quality characteristic in the *i-th* parameter combination, as shown in Table 5.

$$[S_{ij}] = \frac{[x_{ij}] - \min[x_{ij}]}{\max[x_{ij}] - \min[x_{ij}]} \quad (i = 1, 2, \ldots, l; j = 1, 2, \ldots, m) \tag{3}$$

Step 2: Calculate the matrix of the correlation coefficient, eigenvalue, coefficient of determination and eigenvector.

Equation (4) is used to calculate the correlation coefficient of the normalized SN ratio and obtain the matrix of correlation coefficient [R], as shown in Table 6. The matrix of the correlation coefficient, eigenvalue and eigenvector are shown in equation (5). Then, the MINITAB16 software package is used to obtain the eigenvalues and eigenvectors, the eigenvectors are added to the standard column and the coefficient of the determination of each principal component is obtained by equation (6) and the results are shown in Tables 7 and 8.

$$[\gamma_{jj'}] = \frac{\sum_{i=1}^{l}\left(S_{ij} - \overline{S_j}\right)\left(S_{ij'} - \overline{S_{j'}}\right)}{\sqrt{\sum_{i=1}^{l}\left(S_{ij} - \overline{S_j}\right)^2 \sum_{i=1}^{l}\left(S_{ij'} - \overline{S_{j'}}\right)^2}} \tag{4}$$

Figure 9 Temperature curve of the underfilling process

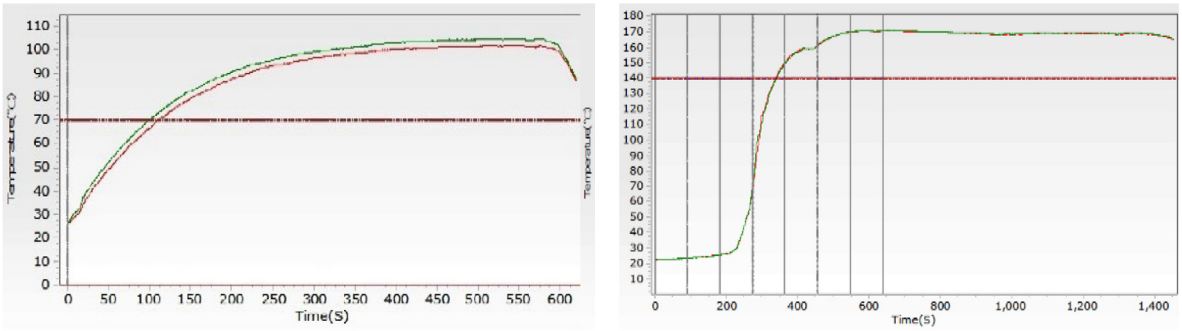

(a) (b)

Notes: (a) Preheating module PCB board temperature (b) Underfill baking and curing

Table 3 Response table of underfilling process parameter design

Control factors	A	B	C	D
Number of solder beads				
Level 1	−28.01	−22.24	−21.72	−25.33
Level 2	−25.37	−21.12	−17.82	−26.54
Level 3	−15.73	−25.76	−29.57	−17.24
Ideal level	A3	B2	C2	D3
Underfill spread distance				
Level 1	−2.14	−2.65	0.10	−1.54
Level 2	0.16	−0.21	−0.79	−1.65
Level 3	0.33	1.21	−0.96	1.55
Ideal level	A3	B3	C1	D3
Underfilling time				
Level 1	−30.03	−29.85	−31.26	−31.48
Level 2	−30.75	−30.24	−32.16	−31.16
Level 3	−33.11	−33.80	−30.47	−31.25
Ideal level	A1	B1	C3	D2

Figure 10 Factor effects of underfilling process parameter design

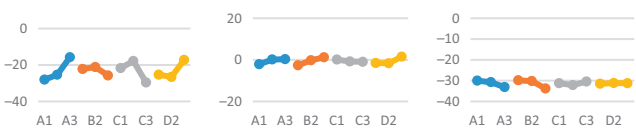

(a) (b) (c)

Notes: (a) Number of solder beads; (b) underfill spread distance; (c) underfilling time

where $\gamma_{jj'}$ is the correlation coefficient between the j-th quality characteristic and the j'-th quality characteristic, $\overline{S_j}$ is the mean of the normalized SN ratio of the experimental group of the j-th quality characteristic and $\overline{S_{j'}}$ is the mean of the normalized SN ratio of the experimental group of the j'-*th* quality characteristic.

$$|[\gamma_{jj'}] - \lambda_p I_{m\times m}|\beta_p = 0, (p = 1, 2, 3, 4) \quad (5)$$

$$C_p = \frac{\lambda_p}{T} \quad (6)$$

Table 4 Original SN ratio matrix

No.	SN_1	SN_2	SN_3
1	−28.19	−4.58	−28.74
2	−24.37	−3.14	−29.69
3	−31.48	1.30	−31.65
4	−13.55	−0.08	−30.11
5	−32.28	−0.91	−29.05
6	−30.27	1.47	−33.08
7	−24.97	−3.28	−30.70
8	−6.69	3.41	−31.98
9	−15.52	0.85	−36.66

Table 5 Normalized SN ratio matrix

RUN	S_{i1}	S_{i2}	S_{i3}
1	0.16	0.00	1.00
2	0.31	0.18	0.88
3	0.03	0.74	0.63
4	0.73	0.56	0.83
5	0.00	0.46	0.96
6	0.08	0.76	0.45
7	0.29	0.16	0.75
8	1.00	1.00	0.59
9	0.66	0.68	0.00

Table 6 Correlation coefficient matrix

	γ_{j1}	γ_{j2}	γ_{j3}
$\gamma_{1j'}$	0.13	0.05	−0.04
$\gamma_{2j'}$	0.05	0.11	−0.06
$\gamma_{3j'}$	−0.04	−0.06	0.10

where λ_p is the eigenvalue of the p-th principal component, $I_{m\times m}$ is an $m \times m$ unit matrix, β_p is the eigenvector corresponding to the λ_p of the p-th principal component, C_p is the coefficients of determination of the p-th principal component and T is the sum of the principal component eigenvalues.

Table 7 Eigenvalues and coefficients of determination

Components	Eigenvalues	Coefficients of determination (%)
First principal component	1.90	64.01
Second principal component	0.40	13.26
Third principal component	0.68	22.73

Table 8 Eigenvector of different principal components

Quality characteristics	Eigenvector First principal component	Second principal component	Third principal component
Number of solder beads	0.51	−0.84	−0.17
Underfill spread distance	0.62	0.23	0.75
Underfilling time	0.59	−0.49	0.64
Standard column	1.726	−1.101	1.222

Step 3: Calculate the principal component score, the main component difference sequence, the gray relational coefficient and the gray relational grade.

The difference sequence among the principal components is obtained by equations (7) and (8), respectively, where Φ_{ip} *is* the p-th principal component for the i-th experimental group, β_{ip} is the eigenvector corresponding to the p-th principal component and $Y_i(p)$ is the principal component of the comparison column of the p-th principal component. Then, equations (9) and (10) are used to, respectively, calculate the gray relational coefficient and grade of each principal component, where $\Delta_{\min} = \min_{\forall i} \min_{\forall p} \|\Delta_i(p)\|$ is the minimum of the difference between the principal components and experimental groups; $\Delta_{\max} = \max_{\forall i} \max_{\forall p} \|\Delta_i(p)\|$ is the maximum of the difference between the principal components and experimental groups, as shown in Table 9.

$$\Phi_{ip} = \sum_{j=1}^{4} \beta_{ip} S_{ij} \tag{7}$$

$$\Delta_i(p) = |Y_0(p) - Y_i(p)|, (i = 1, 2, \cdots, l) \tag{8}$$

$$r_i(p) = \frac{\Delta_{\min} + 0.5\Delta_{\max}}{\Delta_i(p) + 0.5\Delta_{\max}} \tag{9}$$

$$\Gamma_i = \frac{1}{4}\sum_{p=1}^{4} r_i(p) \tag{10}$$

Step 4: Compare the gray relational grade of each experimental group to determine the optimal parameter combination.

The mean gray relational response of each parameter at different levels is calculated. The results show that the optimal underfilling process parameter combination includes 3 dispensing, the "half flow" interval state, 80°C for preheating the module PCB board and an L-shaped dispensing path, which refers to A_2, B_2, C_2, D_3, as shown in Table 10.

3.2 Technique for order preference by similarity to the ideal solution analysis

In this study, the TOPSIS method is used to determine the best and the worst of the multi-quality characteristics. The positive ideal solution and the negative ideal solution are, respectively, used to obtain the closeness of each quality characteristic and the ideal solution as a basis for comparing the quality characteristics (Huang and Chen, 2017; Simsek *et al.*, 2013). The entropy weight method is used to obtain the objective weight and the mean of the repeated measurement is used to calculate the entropy weight. The analysis steps are, as follows:

Step 1: Normalize the obtained SN ratio.

The SN ratio of the measured mass characteristic is normalized by equation (11) to obtain $R = [r_{ij}]_{l\times m}$, which is then a normalized value for the j-th quality characteristic SN ratio under the i-th parameter combination. The result is shown in Table 11.

$$r_{ij} = \frac{x_{ij}}{\sqrt{\sum_{i=1}^{l} x_{ij}^2}}, i = 1, 2, \ldots, l; j = 1, 2, \ldots, m \tag{11}$$

Step 2: Calculate the objective weight with entropy.

The mean of the repeated measurements of each quality characteristic is normalized by equation (12), where x'_{ij} is the mean of the j-th quality characteristics for the i-th parameter combination and r'_{ij} is the normalized average. Then, equation (13) is used to calculate the entropy of each quality

Table 9 Gray relational analysis results

Experimental group	First principal component Φ_{i1}	$\Delta_i(1)$	$r_i(1)$	Second principal component Φ_{i2}	$\Delta_i(2)$	$r_i(2)$	Third principal component Φ_{i3}	$\Delta_i(3)$	$r_i(3)$	Γ_i
1	0.68	1.05	0.46	−0.62	0.48	0.72	0.61	0.61	0.64	0.61
2	0.79	0.94	0.50	−0.65	0.45	0.74	0.65	0.58	0.66	0.63
3	0.85	0.88	0.52	−0.17	0.93	0.50	0.95	0.27	0.91	0.64
4	1.21	0.51	0.70	−0.89	0.21	0.99	0.83	0.39	0.79	0.83
5	0.85	0.87	0.52	−0.36	0.74	0.58	0.96	0.26	0.92	0.67
6	0.78	0.95	0.49	−0.11	0.99	0.48	0.84	0.38	0.80	0.59
7	0.69	1.03	0.47	−0.57	0.53	0.69	0.56	0.67	0.61	0.59
8	1.48	0.24	0.95	−0.90	0.20	1.00	0.96	0.26	0.92	0.96
9	0.76	0.97	0.49	−0.40	0.71	0.59	0.40	0.82	0.54	0.54

Table 10 Response table of principal components analysis and gray relational analysis

Control factors	Dispensing	Interval states	PCB board temperature	Dispensing path
Level 1	0.63	0.67	0.67	0.61
Level 2	0.70	0.75	0.72	0.60
Level 3	0.69	0.59	0.63	0.81
Optimal level	A_2	B_2	C_2	D_3
Difference	0.07	0.16	0.09	0.20
Order	4	2	3	1

Table 11 TOPSIS Analysis results

Experimental group	r_{i1}	r_{i2}	r_{i3}		r'_{i1}	r'_{i2}	r'_{i3}		v_{i1}	v_{i2}	v_{i3}	S_i	S_i	C_i
1	−28.19	−4.58	−28.74		−0.38	−0.60	−0.31		−0.29	−0.07	−0.04	0.25	0.04	0.15
2	−24.37	−3.14	−29.69		−0.33	−0.41	−0.32		−0.25	−0.05	−0.04	0.21	0.09	0.29
3	−31.48	1.30	−31.65		−0.43	0.17	−0.34		−0.32	0.02	−0.04	0.26	0.09	0.27
4	−13.55	−0.08	−30.11		−0.18	−0.01	−0.32		−0.14	−0.00	−0.04	0.09	0.21	0.70
5	−32.28	−0.91	−29.05		−0.44	−0.12	−0.31		−0.33	−0.01	−0.04	0.27	0.06	0.18
6	−30.27	1.47	−33.08		−0.41	0.19	−0.35		−0.31	0.02	−0.04	0.24	0.10	0.29
7	−24.97	−3.28	−30.70		−0.34	−0.43	−0.33		−0.26	−0.05	−0.04	0.22	0.08	0.27
8	−6.69	3.41	−31.98		−0.09	0.45	−0.34		−0.07	0.05	−0.04	0.00	0.29	0.99
9	−15.52	0.85	−36.66		−0.21	0.11	−0.39		−0.16	0.01	−0.05	0.10	0.19	0.66
				W_j	0.75	0.12	0.13	V^-	−0.07	0.05	−0.04			
				e_j	0.88	0.98	0.98	V^+	−0.33	−0.07	−0.05			

characteristic, where e_j is the entropy of the j-th quality characteristic. The objective weight w_j of each quality characteristic is calculated by equation (14) and the result is shown in Table 11.

$$r'_{ij} = \frac{x'_{ij}}{\sum_{i=1}^{l} x'_{ij}} \tag{12}$$

$$e_j = -\frac{1}{\ln l}\sum_{i=1}^{l} r'_{ij}\ln r'_{ij}, i = 1,2,\ldots,l; j = 1,2,\ldots,m \tag{13}$$

$$w_j = \frac{1-e_j}{\sum_{j=1}^{m}(1-e_j)}, i = 1,2,\ldots,l; j = 1,2,\ldots,m \tag{14}$$

Step 3: Calculate the weight matrix, the positive ideal solution and the negative ideal solution.

Suppose that the weights of the m quality characteristics are $W = (w_1, w_2, [\ldots], w_m)$ and $\sum_{j=1}^{m} w_j = 1$, the values of m quality characteristics in matrix $R = [r_{ij}]$ of the SN ratio are normalized by equations (15) and multiplied by their weight, which is the weight matrix V, where v_{ij} is the performance of the i-*th* parameter combination for the *j-th* quality characteristic. The positive and negative ideal solutions are calculated by equations (16) and (17), respectively, as the basis for the relative evaluation between the parameter combinations. The positive ideal solution is composed of the best values of all the quality characteristics; the negative ideal solution is composed of the worst values of all the quality characteristics. The results are shown in Table 11.

$$v_{ij} = r_{ij} \times w_j,\ \mathrm{V} = [v_{ij}]_{l\times m},\ i = 1,2,\ldots,l; j = 1,2,\ldots,m \tag{15}$$

$$V^+ = \{(\max v_{ij}|j \in \mathfrak{J}_1), (\min v_{ij}|j \in \mathfrak{J}_2)|i = 1,2,\ldots,l\} = \{v_1^+, v_2^+, \ldots, v_m^+\} \tag{16}$$

$$V^- = \{(\min v_{ij}|j \in \mathfrak{J}_1), (\max v_{ij}|j \in \mathfrak{J}_2)|i = 1,2,\ldots,l\} = \{v_1^-, v_2^-, \ldots, v_m^-\} \tag{17}$$

Step 4: Calculate the Separation Measure and the closeness of the ideal solution.

Equations (18) and (19) are used to calculate the Euclidean distance of each parameter combination to the positive and negative ideal solution, which refers to the degree of separation (represented by s_i^*, s_i^-, respectively). Then, equation (20) is used to calculate closeness C_i between the experimental combinations and the ideal solution. The results are shown in Table 11.

$$s_i^+ = \sqrt{\sum_{j=1}^{m}\left(v_{ij} - v_j^+\right)^2}, i = 1,2,\ldots,l; j = 1,2,\ldots,m \tag{18}$$

$$s_i^- = \sqrt{\sum_{j=1}^{m}\left(v_{ij} - v_j^-\right)^2}, i = 1,2,\ldots,l; j = 1,2,\ldots,m \tag{19}$$

$$C_i = \frac{s_i^-}{s_i^+ + s_i^-}, i = 1, 2, \ldots, l; 0 \le C_i \le 1 \quad (20)$$

Step 5: Compare the closeness C_i between the experiment combinations and the ideal solution to determine the optimal parameter combination.

The mean gray relational response of each parameter at different levels is calculated. The results show that the optimal underfilling process parameter combination includes 4 dispensing, the "half flow" interval state, 80°C preheating of the module PCB board and an L-shaped dispensing path, which refers to $A_3B_2C_2D_3$, as shown in Table 12.

3.3 Determination of optimal parameter combination

Regarding the interval state, the preheating module PCB board temperature and the dispensing paths of the above two multi-quality analytical methods show the consistent optimal parameter combination, as shown in Table 13. The following is the discussion of the above analysis results. First, the dispensing interval state is "half flow," which can avoid underfilling overflow and the air cavities between the two adhesives to generate air bubbles. The preheating module PCB board temperature is 80°C, which can reduce the viscosity of the underfill, improve its fluidity and prevent premature gelation from generating bubbles or unfilling. At the same time, it can avoid splashing due to low viscosity. The dispensing path is L-shaped, which contributes to the quick filling of the underfill into the bottom of the component, which shortens the completion time of underfilling.

However, regarding the number of dispensing, the principal components/gray relational analysis and TOPSIS show an optimal level of 3 dispensing (15 mg/dispensing) and 4 dispensing (11 mg/dispensing), respectively. The results of the analytical methods are described, as follows: The significance sequences of the parameters (the number of dispensing) in the two analytical methods are 4 and 1, respectively (Tables 10 and 12), indicating that the effect of the parameter on the TOPSIS method result is the most significant; however, the effect of the principal components/gray relational analysis on the experimental results is the least significant. Therefore, considering the analysis results of TOPSIS, the optimal parameter combination includes 4 dispensing (11 mg/dispensing), the "half flow" interval state, 80°C preheating module PCB board temperature and an "L-shaped" dispensing path.

4. Confirmation experiment

A confirmation experiment is performed on the optimal combination of the aforementioned underfilling processes, and three experiments are repeated to determine whether the optimal parameter level combination falls within the confidence interval.

4.1 Confidence interval

First, equation (21) is used to predict the SN ratio under the optimal printing parameter combination, where $\overline{T}$ is the total mean SN of all experimental groups and $\overline{A_3}$, $\overline{B_2}$, $\overline{C_2}$, $\overline{D_3}$ are the mean SN ratio of each control factor at its optimal level. Then, equation (22) is used to calculate the 95% confidence interval (CI) of the predicted SN ratio for each response (Huang, 2015). The measurement results of the characteristics all fall into the confidence interval (Table 14), indicating that the additive mode of each control factor is established and there is no significant interaction among the parameters.

$$SN = \overline{T} + (\overline{A_3} - \overline{T}) + (\overline{B_2} - \overline{T}) + (\overline{C_2} - \overline{T}) + (\overline{D_3} - \overline{T}) \quad (21)$$

$$\mathrm{CI} = \sqrt{F_{\alpha;1;V_2} \times V_e \times \left[\frac{1}{n_{eff}} + \frac{1}{r}\right]}, n_{eff} = \frac{L}{1 + Df^*} \quad (22)$$

where, α is the significance level ($\alpha = 0.05$); v is the degree of freedom of the pooled error variance; V_e is the pooled error variance; *neff* is the effective number of observations; L is the total number of treatments ($L = 9$); Df^* is the sum of the degrees of freedom used to estimate the mean; r is the number of samples for the confirmation experiment ($r = 3$).

5. Conclusion

In the operation process of vehicle electronic products, the solder joints that provide signal transmission are often broken

Table 12 Response table of TOPSIS

Control factors	Dispensing	Interval states	PCB board temperature	Dispensing path
Level 1	0.23	0.37	0.47	0.33
Level 2	0.39	0.48	0.55	0.28
Level 3	0.64	0.40	0.24	0.65
Optimal level	A_3	B_2	C_2	D_3
Difference	0.40	0.12	0.31	0.37
Ranking	1	4	3	2

Table 13 Optimal parameter level combination

	Dispensing	Interval states	PCB board temperature	Dispensing path
Principal components/gray relational analysis	3	Half flow	80°C	L-shaped
TOPSIS	4	Half flow	80°C	L-shaped

Table 14 Confidence intervals of the quality characteristics of the experimental samples

Quality characteristics	Predicted values	95% confidence range	Actual mean values
Number of solder beads	−4.71	−23.74∼14.32	−1.25
Underfill spread distance	4.18	−0.30∼8.66	3.56
Underfilling time	−27.75	−29.08∼−26.42	−29.05

due to thermal cycling and vibration. Therefore, the solder balls are closely surrounded and protected by the underfill through the underfilling process to withstand thermal stress and mechanical external force. The CSP component on a vehicle electronic communication module will be assembled on the system PCB through a second reflow soldering process after the underfilling process. If the underfilling process is defective, it could be followed by a short-circuit fault of the solder balls. In this study, the Taguchi method is used for parameter design. The number of solder beads, the residual underfill spread distance and the completion time of the underfilling are used as the response values to decide the control factors, such as the parameters related to the underfilling process. The L9 orthogonal table is used to schedule and execute the experiment. In addition, the principal components analysis and two multi-quality analytical methods, including gray relational and TOPSIS, are applied to propose the optimal parameter combination, which includes 4 dispensing (11 mg/dispensing), the "half flow" interval status, 80°C preheating module PCB board and an L-shaped dispensing path. It is found from the experiment that the characteristics of the underfill are sensitive, and the fluidity is easily affected by temperature. The Verification test results show that the process parameter combination can minimize the occurrence of solder beads in the underfilling process, reduce the completion time of underfilling and shorten the residual underfill spread distance.

References

Alander, T., Suominen, I., Heino, P. and Ristolainen, E. (2003), "Improving the fatigue life of a bare die flip chip by thinning", *Soldering & Surface Mount Technology*, Vol. 15 No. 3, pp. 8-14.

Cheng, B., Wang, Li, Zhang, Q., Gao, Xia, Xie, X. and Wolfgang, K. (2003), "Reliability and new failure modes of encapsulated flip chip on board under thermal shock testing", *International Conference on Electronic Packaging Technology*, *Shanghai*, pp. 416-421.

Chiang, K.T. and Chang, F.P. (2006), "Optimization of the WEDM process of particle-reinforced material with multiple performance characteristics using grey relational analysis", *Journal of Materials Processing Technology*, Vol. 180 Nos 1/3, pp. 96-101.

Huang, C.Y. (2015), "Innovative parametric design for environmentally conscious adhesive dispensing process", *Journal of Intelligent Manufacturing*, Vol. 26 No. 1, pp. 1-12.

Huang, C.Y. and Chen, C.H. (2017), "Improve electromagnetic compatibility of electronic products with multivariate parametric design – a case with panel PC", *Microelectronics International*, Vol. 34 No. 1, pp. 45-59.

Huang, C.Y., Chen, C.H. and Lin, Y.H. (2016), "A Grey-ANN approach for optimizing the QFN component assembly process for smart phone application", *Soldering & Surface Mount Technology*, Vol. 28 No. 2, pp. 63 -73.

Huang, C.Y., Lin, Y.H. and Tsai, P.F. (2015), "Developing a rework process for underfilled electronics components via integration of TRIZ and cluster analysis", *IEEE Transactions on Components, Packaging and Manufacturing Technology*, Vol. 5 No. 3, pp. 422-438.

Jing Liu, R., Wayne Johnson, E., Yaeger, M., Konarski, L. and Crane, (2003), "Processing and reliability of CSPs with underfill", *IEEE Transactions on Electronics Packaging Manufacturing*, Vol. 26 No. 4, pp. 313-319.

Kuo, J.L., Chao, K.L. and Kuo, C.C. (2010), "Optimal parameter design of solder residue in flip chip process by using Taguchi method'", in *Key Engineering Materials*, Vol. 443, pp. 543-548.

Li, S.H., Huang, C.Y. and Wu, G.D. (2016), "Encapsulation process study and yield model for smart phone manufacturing", *The 17th Asia Pacific Industrial Engineering and Management Systems Conference (APIEMS)*, *Taipei*.

Lu, H.S., Chang, C.K., Hwang, N.C. and Chung, C.T. (2009), "Grey relational analysis coupled with principal component analysis for optimization design of the cutting parameters in high-speed end milling", *Journal of Materials Processing Technology*, Vol. 209 No. 8, pp. 3808-3817.

Nashrudin, M.N., Gan, Z.L., Abas, A., Ishak, M.H.H. and Ali, M.Y.T. (2020), "Effect of hourglass shape solder joints on underfill encapsulation process: numerical and experimental studies", *Soldering & Surface Mount Technology*, Vol. 32 No. 3, pp. 147-156.

Ng, F.C., Abas, M.A. and Abdullah, M.Z. (2019), "Filling efficiency of flip-chip underfill encapsulation process", *Soldering & Surface Mount Technology*, Vol. 32 No. 1, pp. 10-18.

Rangaraj, S., Frutschy, K., Dias, R. and Sankman, B. (2017), "Pressure-Compensated chip attach: a Low-Stress silicon bump reflow process", *IEEE Transactions on Components, Packaging and Manufacturing Technology*, Vol. 7 No. 5, pp. 802-805.

Simsek, B., Iç, Y.T. and Simsek, E.H. (2013), "A TOPSIS-based Taguchi optimization to determine optimal mixture proportions of the high strength self-compacting concrete", *Chemometrics and Intelligent Laboratory Systems*, Vol. 125, pp. 18-32.

Sylvestre, J., Samson, M., Langlois-Demers, D. and Duchesne, E. (2014), "Modeling the flip-chip wetting process", *IEEE Transactions on Components, Packaging and Manufacturing Technology*, Vol. 4 No. 12, pp. 2004-2017.

Vimal, K.E.K., Vinodh, S. and Raja, A. (2017), "Optimization of process parameters of SMAW process using NN-FGRA from the sustainability view point", *Journal of Intelligent Manufacturing*, Vol. 28 No. 6, pp. 1459-1480.

Vincent, M.B. and Wong, C.P. (1999), "Enhancement of underfill encapsulants for flip-chip technology", *Soldering & Surface Mount Technology*, Vol. 11 No. 3, pp. 33-39.

Wu, B. and Han, B. (2018), "Advanced mechanical/optical configuration of Real-Time moiré interferometry for thermal deformation analysis of Fan-Out wafer level package", *IEEE Transactions on Components, Packaging and Manufacturing Technology*, Vol. 8 No. 5, pp. 764-772.

Further reading

He, Y., Moreira, B.E., Overson, A., Nakamura, S.H., Bider, C. and Briscoe, J.F. (2000), "Thermal characterization of an epoxy-based underfillmaterial for flip chip packaging", *Thermochimica Acta*, Vol. 357-358, pp. 1-8.

Straessle, R., Zimmermann, S., Del Carro, L., Zurcher, J., Schlottig, G., Schlottig, G., Achen, A., Hong, G., Poulikakos, D. and Brunschwiler, T. (2018), "Thermally conductive composite material with percolating microparticles applied as underfill", *IEEE Transactions on Components, Packaging and Manufacturing Technology*, Vol. 8 No. 5, pp. 845-850.

NAMICS Corporation.
URL for the source text: www.namics.co.jp/e/

Corresponding author

Chien-Yi Huang can be contacted at:jayhuang@ntut.edu.tw